Inorg. Chem. **2003**, *42*, 2495–2503

Investigating the Stability of the Peroxide Bridge in (μ-oxo)- and Bis(μ-oxo)manganese Clusters

Christopher D. Delfs and Robert Stranger*

Department of Chemistry, Faculty of Science, The Australian National University, Canberra, ACT 0200, Australia

Received September 20, 2002

The stability of the peroxide ligand bridging two manganese ions in the trinuclear oxomanganese complex $[Mn^{III}_3(\mu_3\text{-}O)(\mu\text{-}O_2)(AcO)_2(dien)_3]^{2+}$, one of only two structurally characterized Mn clusters possessing a $\mu_{1,2}$-peroxo bridge, has been investigated using density functional theory. Although the peroxide O–O bond in the related bis(μ-oxo)-bridged complex $[Mn^{IV}_2(\mu\text{-}O)_2(\mu\text{-}O_2)(NH_3)_6]^{2+}$ undergoes spontaneous cleavage upon two-electron reduction to the Mn^{III}_2 dimer, calculations on the model complexes $[Mn^{III}_2(\mu\text{-}O)(\mu\text{-}O_2)(NH_3)_8]^{2+}$ and $[Mn^{III}_2(\mu\text{-}O)(\mu\text{-}O_2)(NH_3)_6(H_2O)_2]^{2+}$, which contain the same μ-oxo-, μ-peroxo-bridged core present in the trimer, indicate that the peroxide bridge remains intact, in agreement with experiment. Its stability can be attributed to a Jahn–Teller distortion resulting in elongation of the axial Mn–N bonds perpendicular to the $Mn_2(\mu\text{-}O)(\mu\text{-}O_2)$ plane which in turn stabilizes the high-spin Mn^{III} oxidation state. However, the difference in the energies of the bridged and cleaved peroxide structures is small (ca. 0.5 eV), the lowest energy structure depending on the nature of the terminal ligands. Calculations on the model trimer complex $[Mn^{III}_3(\mu_3\text{-}O)(\mu\text{-}O_2)(HCO_2)_2(NH_3)_9]^{2+}$ indicate that the energetic differences between the cleaved and uncleaved structures is even smaller (ca. 0.2 eV), and although the peroxo-bridge remains more or less intact, it is likely to be quite facile.

Introduction

The reactions of polynuclear oxomanganese complexes with molecular dioxygen and its oxidized or reduced forms are of intrinsic interest due to their potential relevance to the mechanism of several manganese-containing enzymes such as the oxygen evolving center of photosystem(II), which catalyzes the oxidation of water to dioxygen, and manganese catalase, which catalyzes the disproportionation of hydrogen peroxide into water and dioxygen.[1−6] Since both systems involve magnetically coupled manganese centers, the application of approximate density functional theory, combined with the broken-symmetry approach of Noodleman and coworkers[7,8] in treating oligomeric spin coupled complexes, is yielding valuable insight into the structure and reactivity of the metal sites in these redox-active metalloenzymes.[9−20]

In our ongoing investigations of oxomanganese clusters,[17−20] we recently described the results of a DFT study on the electronic and geometric consequences accompanying two-electron reduction of the model $\mu_{1,2}$-peroxo-bridged complex $[Mn^{IV}_2(\mu\text{-}O)_2(\mu\text{-}O_2)(NH_3)_6]^{2+}$ to $[Mn^{III}_2(\mu\text{-}O)_2(\mu\text{-}O_2)(NH_3)_6]$.[18]

* To whom correspondence should be addressed. E-mail: rob.stranger@anu.edu.au.

(1) Wieghardt, K. *Angew. Chem., Int. Ed. Engl.* **1989**, *28*, 1153.
(2) Pecoraro, V. L.; Baldwin, M. J.; Gelasco, A. *Chem. Rev.* **1994**, *94*, 807.
(3) Manchanda, R.; Brudvig, G. W.; Crabtree, R. H. *Coord. Chem. Rev.* **1995**, *144*, 1.
(4) Dismukes, G. C. *Chem. Rev.* **1996**, *96*, 2909.
(5) Yachandra, V. K.; Sauer, K.; Klein, M. P. *Chem. Rev.* **1996**, *96*, 2927.
(6) Ruttinger, W.; Dismukes, G. C. *Chem. Rev.* **1997**, *97*, 1.
(7) Noodleman, L.; Case, D. A. *Adv. Inorg. Chem.* **1992**, *38*, 423.
(8) Noodleman, L.; Li, J.; Zhao, X.-G.; Richardson, W. H. In *Density Functional Methods in Chemistry and Materials Science*; Springborg, M., Ed.; John Wiley & Sons: New York, 1997.
(9) Zhao, X. G.; Richardson, W. H.; Chen, J. L.; Li, J.; Noodleman, L.; Tsai, H. L.; Hendrickson, D. N. *Inorg. Chem.* **1997**, *36*, 1198.
(10) Brunold, T. C.; Gamelin, D. R.; Stemmler, T. L.; Mandal, S. K.; Armstrong, W. H.; Pennerhahn, J. E.; Solomon, E. I. *J. Am. Chem. Soc.* **1998**, *120*, 8724.
(11) Siegbahn, P. E. M.; Crabtree, R. H. *J. Am. Chem. Soc.* **1999**, *121*, 117.
(12) Brunold, T. C.; Gamelin, D. R.; Solomon, E. I. *J. Am. Chem. Soc.* **2000**, *122*, 8511.
(13) Siegbahn, P. E. M. *Inorg. Chem.* **2000**, *39*, 2913.
(14) Siegbahn, P. E. M. *Theor. Chem. Acc.* **2001**, *105*, 197.
(15) Blomberg, M. R. A.; Siegbahn, P. E. M. *J. Phys. Chem. B* **2001**, *105*, 9375.
(16) Siegbahn, P. E. M. *J. Comput. Chem.* **2001**, *22*, 1634.
(17) McGrady, J. E.; Stranger, R. *J. Am. Chem. Soc.* **1997**, *119*, 8512.
(18) McGrady, J. E.; Stranger, R. *Inorg. Chem.* **1999**, *38*, 550.
(19) Delfs, C. D.; Stranger, R. *Inorg. Chem.* **2000**, 39, 491.
(20) Delfs, C. D.; Stranger, R. *Inorg. Chem.* **2001**, *40*, 3061.

10.1021/ic0205740 CCC: $25.00
Published on Web 03/21/2003

Table 1. Calculated Structural Parameters for the BS and $S = 3$ and 4 States of the Model Complex $[Mn_2(\mu\text{-}O)(\mu\text{-}O_2)(NH_3)_6(H_2O)_2]^{2+}$ Possessing an Intact or Cleaved Peroxo Bridge[a]

	$[Mn_2(\mu\text{-}O)(\mu\text{-}O_2)(NH_3)_6(H_2O)_2]^{2+}$ intact peroxide bridge		$[(MnO)_2(\mu\text{-}O)(NH_3)_6(H_2O)_2]^{2+}$ cleaved peroxide bridge		
	BS	$S = 4$	BS	$S = 3$	expt
Mn−Mn/Å	3.13	3.12	3.37	3.35	3.14(4)
O−O/Å	1.43	1.43	3.17	2.95	1.6(1)
Mn−O/Å	1.81	1.84	1.81	1.84	1.9(1)
$Mn-O_2$/Å	1.85	1.85	1.65	1.65	1.7(1)
$Mn-N_{ax}$/Å	2.46	2.46	2.13	2.13	2.2(1)/2.4(1)
$Mn-N_{eq}$/Å	2.20	2.21	2.22	2.25	2.1(1)
$Mn-O_{eq}$/Å	2.23	2.24	2.57	2.47	2.0(1)
energy/eV	−167.876	−167.714	−168.002	−167.934	
ρ_{spin}(Mn)	±3.64	3.82	±2.31	2.51	
ρ_{spin}(O)	0	0.06	0	−0.06	
ρ_{spin}(O−O)	±0.01	0.09	±0.53	0.49	

[a] The experimental data refer to the corresponding structural parameters in $[Mn_3(\mu_3\text{-}O)(\mu\text{-}O_2)(AcO)_2(dien)_3]^{2+}$.[26] ρ_{spin} refers to the spin density on the relevant atom.

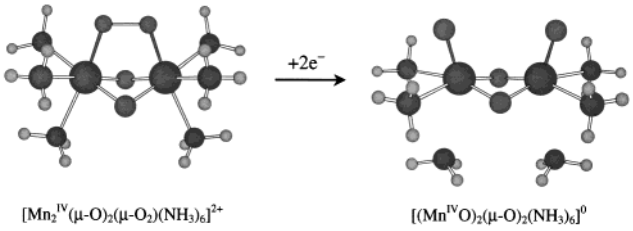

Figure 1. Schematic representation of the structural changes resulting from the two-electron reduction of $[Mn^{IV}_2(\mu\text{-}O)_2(\mu\text{-}O_2)(NH_3)_6]^{2+}$.

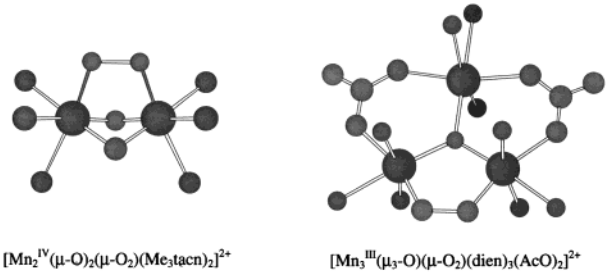

Figure 2. Schematic diagrams of $[Mn^{IV}_2(\mu\text{-}O)_2(\mu\text{-}O_2)(tacn)_2]^{2+}$ and $[Mn^{III}_3(\mu_3\text{-}O)(\mu\text{-}O_2)(AcO)_2(dien)_3]^{2+}$. The ethylene units bridging the N donor atoms are omitted for clarity.

We found that the initial reduction step was metal-based resulting in formally low-spin Mn^{III} centers. This was followed by a structural rearrangement involving transfer of electrons from the minority-spin t_{2g} orbitals on the manganese(III) centers to the peroxo σ^* orbital. As a consequence, the peroxide σ bond was cleaved and the Mn^{IV}_2 core regenerated. Associated with the cleavage of the peroxide σ bond was the formation of a bis(manganyl) $(Mn^{IV}{=}O)_2$ dimer species and dissociation of the amine ligands trans to the peroxo oxygen. A schematic representation of this structural rearrangement is given in Figure 1. Interestingly, for both photosystem(II) and Mn catalase, models have been proposed which involve high-valent Mn=O species as intermediates in the reaction cycle.[14,16,21−24]

Two structurally characterized oxomanganese clusters containing a peroxo bridge are currently known, the dimer complex $[Mn^{IV}_2(\mu\text{-}O)_2(\mu\text{-}O_2)(Me_3tacn)_2]^{2+}$ (Me_3tacn = 1,4,7-trimethyltriazocyclononane)[25] and the trimer $[Mn^{III}_3(\mu_3\text{-}O)(\mu\text{-}O_2)(AcO)_2(dien)_3]^{2+}$ (dien = diethylenetriamine),[26] each of which is shown schematically in Figure 2. In the $[Mn_2(\mu\text{-}O)_2(\mu\text{-}O_2)(Me_3tacn)_2]^{2+}$ dimer, both Mn^{IV} centers are coordinated by two μ-oxo bridging ligands and a $\mu_{1,2}$-peroxo bridge, the remaining three coordination sites being occupied by the N donors of the tridentate ligand Me_3tacn. In the $[Mn^{III}_3(\mu_3\text{-}O)(\mu\text{-}O_2)(AcO)_2(dien)_3]^{2+}$ trimer, however, each Mn^{III} center is coordinated by a tridentate dien ligand in a *mer* fashion with the remaining coordination sites being occupied by the central μ_3-oxo ligand and either acetate or peroxo bridges.

Some relevant structural parameters for the trimer complex are given in Table 1. One intriguing aspect of this structure is that the peroxo O−O distance of 1.6(1) Å is quite long compared to 1.46 Å in $[Mn^{IV}_2(\mu\text{-}O)_2(\mu\text{-}O_2)(Me_3tacn)_2]^{2+}$. At this distance, coupled with the relatively large uncertainty in bond length, it is difficult to ascertain whether the peroxo bridge is still intact. Assuming it is intact, it is important, given the results of our previous calculations on $[Mn^{IV}_2(\mu\text{-}O)_2(\mu\text{-}O_2)(NH_3)_6]^{2+}$ where the peroxo O−O bond is cleaved on reduction to Mn^{III}_2, to understand what structural or electronic variations lead to the stabilization of the peroxo bridge across the two Mn^{III} ions in the trimer. Accordingly, we now report the results of a series of DFT calculations investigating the electronic structure of model dimer and trimer complexes which contain the $[Mn^{III}_2(\mu\text{-}O)(\mu\text{-}O_2)]$ core present in the structurally characterized trimer compound.

Computational Details

The calculations described here were performed using the 1999 version of the Amsterdam Density Functional program[27] running on Linux-based Pentium III 600 MHz computers. For the model dimers $[Mn^{III}_2(\mu\text{-}O)(\mu\text{-}O_2)(NH_3)_8]^{2+}$ and $[Mn^{III}_2(\mu\text{-}O)(\mu\text{-}O_2)(NH_3)_6(H_2O)_2]^{2+}$, triple-$\zeta$ basis sets (type IV) were employed for the

(21) Sakiyama, H.; Tamaki, H.; Kodera, M.; Matsumoto, N.; Okawa, H. *J. Chem. Soc., Dalton Trans.* **1993**, 591.
(22) Sakiyama, H.; Okawa, H.; Suzuki, M. *J. Chem. Soc., Dalton Trans.* **1993**, 3823.
(23) Sakiyama, H.; Okawa, H.; Isobe, R. *J. Chem. Soc., Chem Commun.* **1993**, 822.
(24) Limburg, J.; Szalai, V. A.; Brudvig, G. W. *J. Chem. Soc., Dalton Trans.* **1999**, 1353.
(25) Bossek, U.; Weyhermuller, T.; Wieghardt, K.; Nuber, B.; Weiss, J. *J. Am. Chem. Soc.* **1990**, *112*, 6387.
(26) Bhula, R.; Gainsford, G. J.; Weatherburn, D. C. *J. Am. Chem. Soc.* **1988**, *110*, 7550.

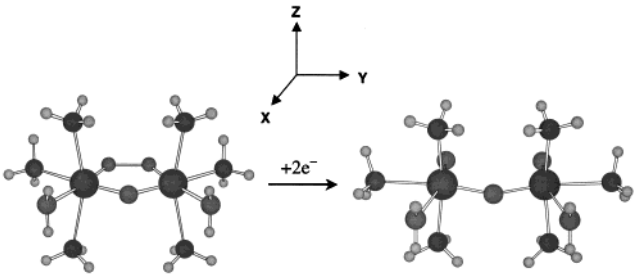

Figure 3. Schematic representation of the structural changes resulting from the two-electron reduction of $[Mn^{III}_2(\mu\text{-}O)(\mu\text{-}O_2)(NH_3)_6(H_2O)_2]^{2+}$.

manganese and oxygen atoms belonging to the bridging oxo and peroxo groups. For the nitrogen, oxygen, carbon, and hydrogen atoms belonging to the terminal ligands, double-ζ basis sets (type III) were used which included a polarization function. The frozen core approximation was employed with the 1s orbital for nitrogen and oxygen and orbitals up to and including 3p for manganese, being treated as frozen. All calculations included the Vosko, Wilk, and Nusair (VWN) local density functional[28] and the gradient corrections for the exchange (Becke)[29] and correlation (Perdew).[30] Geometry optimizations used the algorithm of Versluis and Ziegler.[31] The default values for the convergence criteria of *TolE* = 0.001 hartrees (energy), *TolG* = 0.01 hartrees/Å (gradients), *TolR* = 0.01 Å (coordinates), and *TolA* = 0.5° (angles) were used along with default value of *accint* = 4.0 for the numerical integration accuracy. Calculations on the model complexes employed C_{2v} point group symmetry except for the broken symmetry (BS) calculations which were undertaken in C_s symmetry but with the added restriction that the molecular structure maintained C_{2v} symmetry. Potential energy curves for the BS state of the model dimers were generated by incrementing the peroxo O−O distance in 0.2 Å steps but otherwise optimizing all other geometrical variables. Calculations on the model trimer $[Mn_3(\mu_3\text{-}O)(\mu\text{-}O_2)(\mu\text{-}O_2CH)_2(NH_3)_9]^{2+}$ employed standard type IV basis sets on the manganese and the bridging oxo and peroxo atoms and type III basis sets on all other atoms. Geometry optimizations were undertaken using pseudo-C_2 symmetry, but in all other respects the computational details were the same as those described above for the model dimer complexes. Magnetic exchange constants, *J*, for the model dimers were calculated using spin projection methods.[7,8]

Results and Discussion

Description of Model Complexes. To reduce the computational effort but still retain the essential features of the peroxo-bridged manganese core present in the trimer, we initially employed the model complex, $[Mn^{III}_2(\mu\text{-}O)(\mu\text{-}O_2)(NH_3)_6(H_2O)_2]^{2+}$, shown in Figure 3. In this dimer model, only the Mn ions bridged by the peroxide ligand are included. Each dien ligand is replaced with three NH_3 groups, and the oxygen donor belonging to the acetate ligand which bridges to the third Mn ion is replaced by a water ligand. For the purpose of comparison with earlier studies,[18] we have also undertaken calculations on the model complex $[Mn^{III}_2(\mu\text{-}O)(\mu\text{-}O_2)(NH_3)_8]^{2+}$, where both H_2O groups are replaced by ammonia ligands.

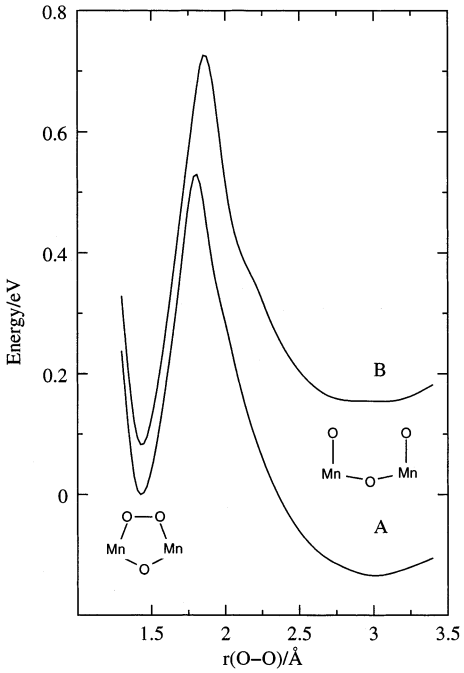

Figure 4. Variation in total energy as a function of the peroxo O−O distance for $[Mn^{III}_2(\mu\text{-}O)(\mu\text{-}O_2)(NH_3)_6(H_2O)_2]^{2+}$ (A) and $[Mn^{III}_2(\mu\text{-}O)(\mu\text{-}O_2)(NH_3)_8]^{2+}$ (B).

Calculations were also performed on the model trimer complex $[Mn^{III}_3(\mu_3\text{-}O)(\mu\text{-}O_2)(\mu\text{-}O_2CH)_2(NH_3)_9]^{3+}$, in which each dien ligand in the observed structure has been replaced with three ammonia ligands as shown in Figure 2. Although the observed structure has no symmetry, the bond distances and angles around the Mn ions in the model complex were restricted such that the molecular geometry approximated C_2 symmetry. The pseudo-C_2 rotation axis passes through the central μ_3-O atom and bisects the peroxo O−O bond. An alternative and perhaps more obvious choice is C_s symmetry, where the mirror plane contains the three Mn ions, the μ_3-O atom, and peroxo bridges. However, this choice of symmetry imposes considerable structural inflexibility as the acetate and peroxide groups are forced to remain planar. This in turn forces the peroxide O atoms into close contact thus limiting the possibility of partial or complete cleavage of the peroxo bridge. In contrast, the pseudo-C_2 symmetry described above allows the acetate and peroxo ligands to buckle out of the plane defined by the three Mn ions and the central μ_3-O unit.

Dimer Models. The calculated energies for the antiferromagnetic BS state of the model dimer complexes $[Mn^{III}_2(\mu\text{-}O)(\mu\text{-}O_2)(NH_3)_6(H_2O)_2]^{2+}$ and $[Mn^{III}_2(\mu\text{-}O)(\mu\text{-}O_2)(NH_3)_8]^{2+}$ are plotted as a function of the peroxo O−O distance in Figure 4. It is immediately apparent that the potential energy

(27) Baerends, E. J.; A Bérces; Bo, C.; Boerrigter, P. M.; Cavallo, L.; Deng, L.; Dickson, R. M.; Ellis, D. E.; Fan, L.; Fischer, T. H.; Fonseca Guerra, C.; van Gisbergen, S. J. A.; Groeneveld, J. A.; Gritsenko, O. V.; Harris, F. E.; van den Hoek, P.; Jacobsen, H.; van Kessel, G.; Kootstra, F.; van Lenthe, E.; Osinga, V. P.; Philipsen, P. H. T.; Post, D.; Pye, C.; Ravenek, W.; Ros, P.; Schipper, P. R. T.; Schreckenbach, G.; Snijders, J. G.; Sola, M.; Swerhone, D.; te Velde, G.; Vernooijs, P.; Versluis, L.; Visser, O.; van Wezenbeek, E.; Wiesenekker, G.; Wolff, S. K.; Woo, T. K.; Ziegler, T. *Amsterdam Density Functional*, 1999 ed.; 1999.
(28) Vosko, S. H.; Wilk, L.; Nusair, M. *Can. J. Phys.* **1980**, *58*, 1200.
(29) Becke, A. D. *Phys. Rev. A* **1988**, *38*, 3098.
(30) Perdew, J. P. *Phys. Rev. B* **1986**, *33*, 8822.
(31) Versluis, L.; Ziegler, T. J. *J. Chem. Phys.* **1988**, *88*, 322.10.

curves have two minima. The first occurs at $r(O-O) \approx 1.4$ Å and the second when the peroxo bridge is cleaved at $r(O-O) \approx 3.0$ Å. For $[Mn^{III}_2(\mu\text{-}O)(\mu\text{-}O_2)(NH_3)_6(H_2O)_2]^{2+}$, the most stable structure has the O−O bond cleaved whereas, for $[Mn^{III}_2(\mu\text{-}O)(\mu\text{-}O_2)(NH_3)_8]^{2+}$, the peroxide bond is intact with $r(O-O) \approx 1.4$ Å. The energy difference between the bridged and cleaved forms is small, approximately 0.1 eV, but importantly, an energy barrier of approximately 0.6 eV separates the cleaved and uncleaved structures in both complexes. Although, on the basis of Figure 4, the nature of the terminal ligands appears to have only a minor influence on the overall energetics, they play a pivotal role in determining whether the global minimum corresponds to a cleaved or intact peroxo O−O bond. In contrast, the number of oxo bridges, which in turn dictates the number of terminal ligands on the Mn centers, has a dramatic effect on the energetics as can be appreciated by comparing the structures of $[Mn^{III}_2(\mu\text{-}O)_2(\mu\text{-}O_2)(NH_3)_6]^0$ and $[Mn^{III}_2(\mu\text{-}O)(\mu\text{-}O_2)(NH_3)_6(H_2O)_2]^{2+}$ shown in Figures 1 and 3, respectively. In the discussion to follow, we examine the structures corresponding to the cleaved and uncleaved BS minima observed in Figure 4.

Uncleaved Peroxo Bridge Structure. Structural parameters from the geometry optimization of the BS and $S = 4$ states of the model complex $[Mn^{III}_2(\mu\text{-}O)(\mu\text{-}O_2)(NH_3)_6(H_2O)_2]^{2+}$, corresponding to the BS minimum at $r(O-O) \approx 1.4$ Å in Figure 4, are given in Table 1 along with the relevant data from the X-ray structure of $[Mn_3(\mu_3\text{-}O)(\mu\text{-}O_2)(AcO)_2(dien)_3]^{2+}$.[26] The calculated structures for the BS and $S = 4$ states are very similar indicating the Mn centers are high spin and only weakly coupled. Except for the $Mn-N_{ax}$ and $Mn-O_{eq}$ distances, a comparison of the observed and calculated bond distances reveals that most of the calculated values are within two standard deviations of experiment and generally in the range of distances known for other dimers containing $[Mn^{III}_2(\mu\text{-}O)_2]^{n+}$ or $[Mn^{III}_2(\mu\text{-}O)(RCO_2)_2]^{n+}$ cores.[32−39] It seems reasonable to attribute the poorer agreement between the model and the X-ray structure for the $Mn-O_{eq}$ distance to differences between carboxylate- and water-based oxygen donors.

The imposition of C_{2v} symmetry on the model complex ensures that all the calculated $Mn-N_{ax}$ distances are identical. In contrast, the lower symmetry of the X-ray structure allows for two different $Mn-N_{ax}$ distances, 2.2(1) and 2.4(1) Å, on each Mn center. The calculated $Mn-N_{ax}$ distance of 2.46 Å is long but not unexpected for high-spin Mn^{III}, which is Jahn−Teller active, resulting in axial elongation if the d_{z^2} orbital is occupied. In previous calculations on $[Mn^{III}_2(\mu\text{-}O)_2(NH_3)_8]^{2+}$, the $Mn-N_{ax}$ distance was determined to be 2.50 Å.[17] Reported structures of dimers with a $[Mn_2(\mu\text{-}O)_2]^{2+}$ core have $Mn-N_{ax}$ distances in the range 2.32−2.42 Å. However, in most of these cases the axial N donors are members of aromatic systems and therefore π interactions with the Mn ion are likely to lead to shorter Mn−N distances. The calculated peroxo O−O distance of 1.43 Å is well short of 1.6 Å observed in $[Mn_3(\mu_3\text{-}O)(\mu\text{-}O_2)(AcO)_2(dien)_3]^{2+}$ but compares well with the value of 1.46 Å found for $[Mn^{IV}_2(\mu\text{-}O)_2(\mu\text{-}O_2)(Me_3tacn)_2]^{2+}$.[25]

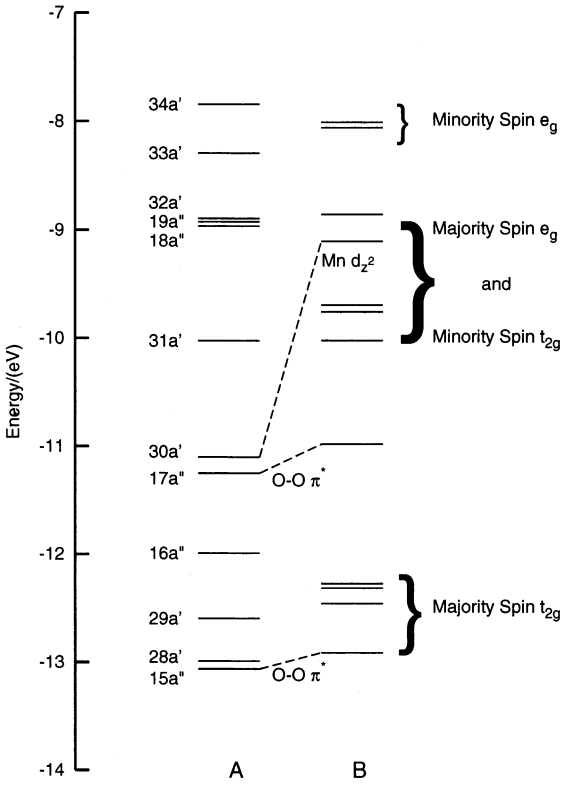

Figure 5. Relative energies of the molecular orbitals near the HOMO and LUMO levels in the broken-symmetry state for $[Mn^{III}_2(\mu\text{-}O)(\mu\text{-}O_2)(NH_3)_6(H_2O)_2]^{2+}$ (A) and $[Mn^{IV}_2(\mu\text{-}O)_2(\mu\text{-}O_2)(NH_3)_6]^{2+}$ (B).

The relative energies of the spin-up molecular orbitals near the HOMO−LUMO gap for the BS state of the model complex $[Mn^{III}_2(\mu\text{-}O)(\mu\text{-}O_2)(NH_3)_6(H_2O)_2]^{2+}$ are shown in Figure 5, and their compositions are given in Table 2. The corresponding spin-down orbitals are not shown but are degenerate with their spin-up counterparts. As found in other calculations on Mn systems containing μ-oxo and μ-peroxo bridges, the interactions between the metal centers and the bridging ligands are highly covalent.[9−20] Accordingly, in the discussion that follows, the labeling of orbitals as either t_{2g}, e_g, or π^* is meant solely as an indication of the major contributors to a molecular orbital.

Figure 5 reveals that the π^* orbitals (28A′ and 17A″) of the peroxo bridge are similar in energy to the t_{2g} orbitals of

(32) Wieghardt, K.; Bossek, U.; Ventur, D.; Weiss, J. *J. Chem. Soc., Chem. Commun.* **1985**, 347.
(33) Bossek, U.; Wieghardt, K.; Nuber, B.; Weiss, J. *Inorg. Chim. Acta* **1989**, *165*, 123.
(34) Wu, F.-J., Jr.; D. M. K.; Hagen, K. S.; Nyman, P. D.; Debrunner, P. G.; Vankai, V. A. *Inorg. Chem.* **1990**, *29*, 5174.
(35) Goodson, P. A.; Oki, A. R.; Glerup, J.; Hodgson, D. J. *J. Am. Chem. Soc.* **1990**, *112*, 6248.
(36) Vincent, J. P.; Tsai, H.; Blackman, A. G.; Wang, S.; Boyd, P. D. W.; Folting, K.; Huffman, J. C.; Lobkovsky, E. B.; Hendrickson, D. N.; Christou, G. *J. Am. Chem. Soc.* **1993**, *115*, 12353.
(37) Glerup, J.; Goodson, P. A.; Hazell, A.; Hazell, R.; Hodgson, D. J.; McKenzie, C. J.; Michelsen, K.; Rychlewska, U.; Toftlund, H. *Inorg. Chem.* **1994**, *33*, 4105.
(38) Bossek, U.; Hummel, H.; Weyhermuller, T.; Wieghardt, K.; Russell, S.; Vanderwolf, L.; Kolb, U. *Angew. Chem., Int. Ed. Engl.* **1996**, *35*, 1552.
(39) Corbella, M.; Costa, R.; Ribas, J.; Fries, P. H.; Latour, J.-M.; Öhrström, L.; Solans, X.; Rodríguez, V. *Inorg. Chem.* **1996**, *35*, 1857.

Table 2. Mulliken Decomposition of the Upper Valence Molecular Orbitals for the Broken-Symmetry States of the Model Complexes $[Mn_2(\mu\text{-}O)(\mu\text{-}O_2)(NH_3)_6(H_2O)_2]^{2+}$ and $[(MnO)_2(\mu\text{-}O)(NH_3)_6(H_2O)_2]^{2+}$ [a]

MO	energy/ eV	occ	Mn_1	Mn_2	O	O_p	O_w	N
			$[Mn_2(\mu\text{-}O)(\mu\text{-}O_2)(NH_3)_6(H_2O)_2]^{2+}$					
34A′	−7.845	0	1 d_{xy}	61 d_{xy}	9	10	0	1
33A′	−8.293	0	0	81 d_{z^2}	0	3	0	8
32A′	−8.895	0	19 d_{xy}, $d_{x^2-y^2}$	49 $d_{x^2-y^2}$	17	7	0	0
19A″	−8.927	0	0	84 d_{yz}, d_{xz}	11	1	0	0
18A″	−8.965	0	0	81 d_{xz}, d_{yz}	0	16	0	0
31A′	−10.026	0	34 d_{xy}	39 $d_{x^2-y^2}$, d_{xy}	2	15	0	2
30A′	−11.100	2	57 d_{z^2}	1 $d_{x^2-y^2}$	3	10	0	19
17A″	−11.250	2	21 d_{xz}	7 d_{xz}	0	64	0	1
16A″	−11.991	2	55 d_{yz}	7 d_{yz}	30	0	0	3
29A′	−12.596	2	54 $d_{x^2-y^2}$	8 $d_{x^2-y^2}$	28	0	0	0
28A′	−12.990	2	18 d_{xy}, d_{z^2}	4 d_{xy}, d_{z^2}	3	62	5	0
15A″	−13.062	2	63 d_{xz}	3 d_{xz}	0	26	0	0
			$[(MnO)_2(\mu\text{-}O)(NH_3)_6(H_2O)_2]^{2+}$					
35A′	−7.658	0	2	44 $d_{x^2-y^2}$	4	17	0	0
34A′	−8.283	0	8 $d_{x^2-y^2}$, d_{xy}	49 d_{xy}	10	19	0	1
33A′	−8.540	0	15 $d_{x^2-y^2}$	50 d_{z^2}	5	11	0	9
32A′	−8.863	0	32 $d_{x^2-y^2}$	29 d_{xy}, $d_{x^2-y^2}$, d_{z^2}	0	27	0	1
19A″	−8.879	0	0	62 d_{xz}	1	33	0	0
18A″	−9.726	0	2 d_{yz}	80 d_{yz}	14	0	0	0
31A′	−9.829	0	58 d_{z^2}	8 d_{xy}, d_{z^2}	6	8	0	15
30A′	−10.683	2	45 d_{xy}	1 d_{xy}	2	42	0	3
17A″	−10.916	2	43 d_{xz}	1 d_{yz}	0	50	0	2
16A″	−12.247	2	56 d_{yz}	10 d_{yz}	23	3	0	2

[a] Only spin-up orbitals are listed. Atomic orbital contributions to the molecular orbitals are listed in order of weighting. O, O_p, and O_w refer to the oxo, peroxo, and water oxygen atoms, respectively.

the Mn^{III} ions, resulting in significant mixing between these levels. As shown in Figure 6a, the HOMO (30a′↑) is highly localized on one side of the dimer (Mn_1:Mn_2 = 57:1) and consists mainly of the majority-spin d_{z^2} orbital on Mn_1 with some contributions from 2p orbitals on the axial N donors as well as smaller contributions from the bridging oxo and peroxo ligands. The calculated structure is consistent with the occupation of the d_{z^2} orbital which results in the Mn−N_{ax} distance being much larger the Mn−N_{eq} distance due to a Jahn−Teller effect. That the d_{z^2} orbital is lower in energy than $d_{x^2-y^2}$ is a consequence of the stronger ligand field exerted by the oxo and peroxo ligands relative to the axial N donors.

The spin density for the BS and $S = 4$ states given in Table 1 is derived from a Mulliken population analysis and indicates high-spin configurations for both Mn^{III} ions. It is important to note that, in the BS formalism, the spin-up and spin-down density is free to localize on opposite metal centers or to delocalize across both Mn ions. Thus, there is no restriction that forces the electrons into a configuration corresponding to either high-spin or low-spin Mn^{III}. The compositions of the predominantly Mn-based orbitals 29A′ and 16A″ in Table 2 reveal that the major magnetic interactions, as measured by the extent of delocalization of the spin-up electron density over both Mn centers, occur via the symmetric $J_{x^2-y^2/x^2-y^2}$ and $J_{yz/yz}$ exchange pathways involving overlap of t_{2g}-based Mn orbitals with pπ orbitals on the bridging oxo ligand. Using spin projection methods[7,8] and the Heisenberg spin Hamiltonian, $H = -2JS_1 \cdot S_2$, where S_1 and S_2 are the spins on metal centers 1 and 2, respectively, the exchange coupling constant, J, can be calculated from the energies of the broken symmetry, BS, and maximum spin, S_{max}, states using the expression

$$-J = \frac{E(S_{max}) - E_{BS}}{{S_{max}}^2}$$

Using the above equation, both model complexes $[Mn^{III}{}_2(\mu\text{-}O)(\mu\text{-}O_2)(NH_3)_6(H_2O)_2]^{2+}$ and $[Mn^{III}{}_2(\mu\text{-}O)(\mu\text{-}O_2)(NH_3)_8]^{2+}$ are predicted to be antiferromagnetic with calculated exchange coupling constants of $-J = 82$ and 97 cm^{-1}, respectively.

The LUMO (31a′) shown in Figure 6B is significantly delocalized across both metal centers (Mn_1:Mn_2 = 34:39) and comprises a mixture of the majority-spin e_g-based d_{xy} orbital on Mn_1 and the minority-spin t_{2g}-based $d_{x^2-y^2}$ orbital on Mn_2, as well as contributions from the peroxo bridging ligand. The composition of this orbital is important as it is this level which is occupied on further reduction of the metal centers. The cross delocalization arising from the mixing of the majority spin e_g orbitals on one Mn center with the minority-spin t_{2g} orbitals on the other has been noted in calculations on several mixed-valence oxomanganese dimers.[12,17,20] In those studies, the cross delocalization resulted in a ground state which can be described as a mixture of Mn^{IV} magnetically coupled with high-spin Mn^{III} and low-spin Mn^{III} magnetically coupled with Mn^{IV}. On further reduction, the additional electrons in the BS state are found to occupy the 31a′↑ and 31a′↓ levels which are principally minority-spin t_{2g} orbitals. Thus, the initial reduction step for which the peroxide bridge is still intact gives rise to Mn^{II} ions of intermediate spin ($S = 3/2$). However, as shown schematically in Figure 3, the structural relaxation following the initial reduction step results in the spontaneous cleavage of the peroxide bridge to form $[(MnO)_2(\mu\text{-}O)(NH_3)_6(H_2O)_2]^0$, analogous to the two-electron reduction of $[Mn^{IV}{}_2(\mu\text{-}O)_2(\mu\text{-}O_2)(NH_3)_6]^{2+}$.[18]

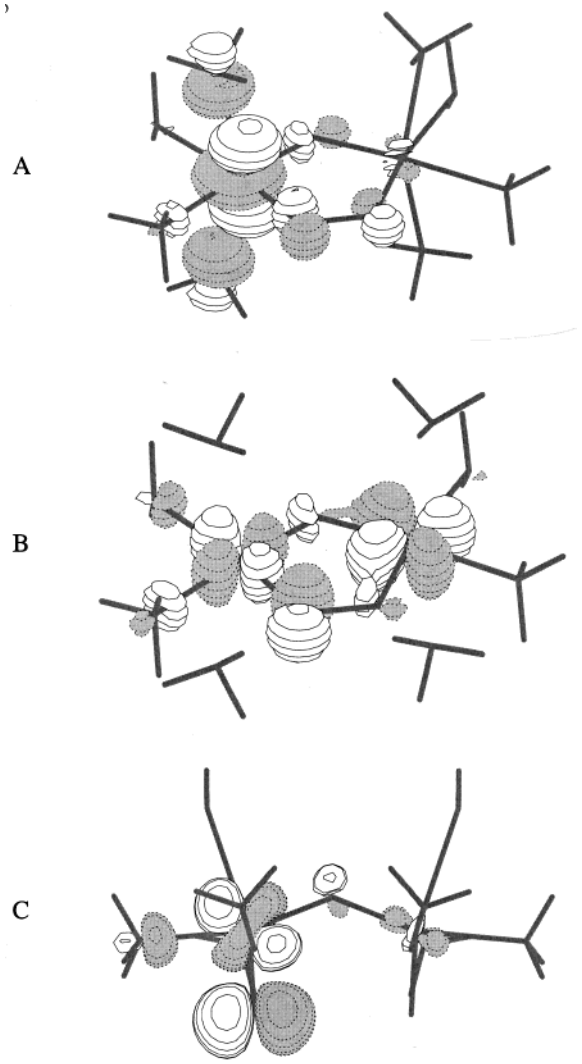

Figure 6. Pseudo-three-dimensional plot of the 30A′ HOMO (A) and 31A′ LUMO (B) in the broken-symmetry calculation of $[Mn^{III}_2(\mu\text{-}O)(\mu\text{-}O_2)(NH_3)_6(H_2O)_2]^{2+}$ and the 30A′ HOMO (C) in the broken-symmetry calculation of $[(MnO)_2(\mu\text{-}O)(NH_3)_6(H_2O)_2]^{2+}$. The coordinate system used to generate the plots is the same as that shown in Figure 3.

Cleaved Peroxo Bridge Structure. Parameters describing the structure of the model dimer $[(MnO)_2(\mu\text{-}O)(NH_3)_6(H_2O)_2]^{2+}$, corresponding to the BS minimum at $r(O-O) \approx 3.0$ Å in Figure 4, are given in Table 1. Unfortunately, there are no experimental structures with which direct comparisons can be made. However, there are a few examples of monomeric complexes containing a $Mn^{V}{=}O$, moiety all of which have very short Mn−O distances (1.55−1.56 Å).[40,41]

Some of the differences between the two structural minima of our model system are similar to the changes in geometry found for the two-electron reduction of $[Mn^{IV}_2(\mu\text{-}O)_2(\mu\text{-}O_2)(NH_3)_6]^{2+}$.[18] The single biggest structural change in the model complex involves the peroxo oxygens. Most notably, the O−O distance, which has increased by 1.74 Å, indicates that the peroxide bridge is cleaved. In addition, the $Mn-O_2$ distance has contracted by approximately 0.2 Å, consistent with the formation of a Mn═O moiety. Another important difference is that the $Mn-N_{ax}$ distance has decreased by more than 0.3 Å compared to the peroxo-bridged structure, with the result that it is now comparable to the $Mn-N_{eq}$ distance. Clearly there is no longer any significant Jahn−Teller distortion along the $Mn-N_{ax}$ axis. Instead, the $Mn-O_{eq}$ distance, which is trans to the Mn═O moiety, has increased by more than 0.3 Å. In our earlier studies on $[Mn^{IV}_2(\mu\text{-}O)_2(\mu\text{-}O_2)(NH_3)_6]^{2+}$, the NH_3 ligand trans to the peroxide oxygen was found to dissociate completely from the dimer, due to the trans influence of the peroxo ligand, resulting in a square pyramidal stereochemistry with the oxo ligand in the axial position. At the calculated $Mn-O_{eq}$ distance of 2.57 Å, the water ligand is only weakly bound to the Mn ion. This was confirmed by additional calculations which indicated that only 1 eV is required to completely remove both water ligands. Finally, the 0.25 Å increase in the Mn−Mn distance is associated with an increase of approximately 18° in the Mn−O−Mn angle.

From the composition of the predominantly Mn-based orbitals given in Table 2, only the 16A″ level exhibits reasonable delocalization (Mn_1:Mn_2 = 56:10) across both Mn centers. Consequently, in the cleaved structure only the symmetric $J_{yz/yz}$ exchange pathway involving the bridging oxo ligand is significant. Using spin projection methods,[7,8] the cleaved peroxo bridge form of $[Mn^{III}_2(\mu\text{-}O)(\mu\text{-}O_2)(NH_3)_6(H_2O)_2]^{2+}$ is also predicted to be antiferromagnetic but the calculated exchange coupling constant of $-J = 61$ cm^{-1} is approximately 20 cm^{-1} smaller than that calculated for $[Mn^{III}_2(\mu\text{-}O)(\mu\text{-}O_2)(NH_3)_6(H_2O)_2]^{2+}$. This reduction can be accounted for on the basis that the symmetric $J_{x^2-y^2/x^2-y^2}$ pathway operating in the uncleaved complex is effectively eliminated due to the extensive involvement of the Mn $d_{x^2-y^2}$ orbitals in forming the strongly covalent Mn═O bonds, apparent from the composition of the 32A′ orbital in Table 2.

In our previous study on the two-electron reduction of $[Mn^{IV}_2(\mu\text{-}O)_2(\mu\text{-}O_2)(NH_3)_6]^{2+}$, it was found that the O−O bond cleavage and Mn═O double bond formation was accompanied by the regeneration of the stable $(t_{2g})^3$ configuration on each of the Mn ions. Hence a formal oxidation state of 4+ on the Mn in the reduced complex was a better description of the electronic configuration than 3+. Likewise, from Table 1, the change in spin density from 3.64 to 2.31 on the Mn in the BS state of the current model complex $[Mn^{III}_2(\mu\text{-}O)(\mu\text{-}O_2)(NH_3)_6(H_2O)_2]^{2+}$ reflects the oxidation of the Mn centers from 3+ to 4+ when the peroxo bridge is cleaved. However, there is also a large amount of unpaired spin (approximately 0.5 electrons) on each of the peroxo oxygens, consistent with a highly covalent interaction between these atoms and the Mn ions. The large metal−ligand covalency is highlighted in Figure 6C which shows that the 30a′↑ HOMO is composed of approximately equal proportions of Mn d_π and peroxo O p_π orbitals. Thus, a more accurate description of the cleaved structure is $[(Mn^{IV}O)_2(\mu\text{-}O)(NH_3)_6(H_2O)_2]^{2+}$, where each MnO unit is associated with three unpaired electrons spins. This description of the $Mn-O_{peroxo}$ bonding in the BS state is confirmed from the

(40) Collins, T. J.; Powell, R. D.; Slebodnick, C.; Uffelman, E. S. *J. Am. Chem. Soc.* **1990**, *112*, 899.
(41) MacDonnell, F. M.; Fackler, N. L. P.; Stern, C.; Ohalloran, T. V. *J. Am. Chem. Soc.* **1994**, *116*, 7431.

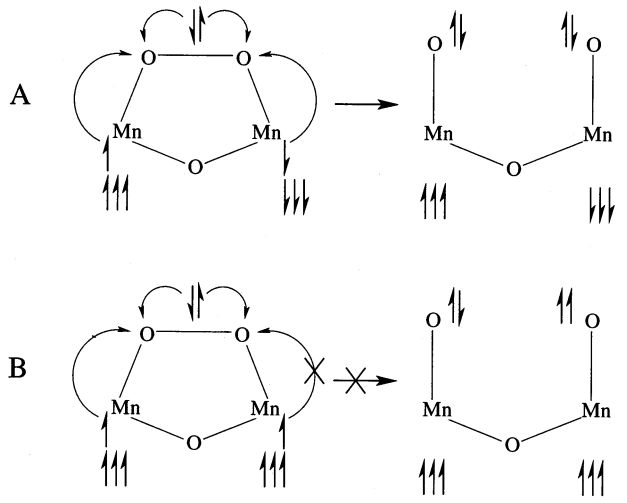

Figure 7. Schematic representation of the electron rearrangement accompanying peroxo O−O cleavage in the broken-symmetry state (A) and $S = 4$ state (B) of $[Mn^{III}_2(\mu\text{-}O)(\mu\text{-}O_2)(NH_3)_6(H_2O)_2]^{2+}$.

close agreement between the calculated structures for the BS and $S = 3$ states, the latter being derived from ferromagnetic coupling of two $S = 3/2$ metal centers.

Attempts to locate an optimized structure for the $S = 4$ state with a cleaved peroxo bridge unit, similar to the geometry of the BS state, were unsuccessful. All $S = 4$ geometry optimizations that were started with a large r(O−O) relaxed to the structure described in Table 1. The reason for this becomes obvious when the nature of the electronic rearrangement accompanying the O−O cleavage is considered. It is instructive to first examine the electron rearrangement in the BS state as depicted schematically in Figure 7a. In the simplest description, we assign formal oxidation states of 4+ and 2−, respectively, to the Mn and peroxo O atoms in the cleaved structure. For the peroxide bridge to cleave, the electrons in the O−O σ bond must localize onto the peroxo O atoms (the spin-down electron going to O_1 and the spin-up electron going to O_2). A second electron of opposite spin is also transferred to the peroxo O atoms from the Mn. That is, a spin-up electron is transferred from Mn_1 to O_1 and a spin-down electron from Mn_2 to O_2. The resulting configuration can be considered as two antiferromagnetically coupled Mn^{4+} (d^3) ions with an additional electron pair on each peroxo O center. As shown in Figure 7b for the $S = 4$ state of the bridged structure, all the electrons on the Mn centers are aligned spin up. For the peroxide bridge to cleave, the electrons in the O−O σ bond must again localize on the peroxo O atoms as described above for the BS state. However, now there are no spin-down electrons on Mn_2 which can be transferred to O_2 to pair with the spin-up electron from the O−O σ bond. Since transfer of a spin-up electron from Mn_2 to O_2 results in a configuration that violates the Pauli exclusion principal, a cleaved peroxo-bridge structure in the $S = 4$ state is unstable. Instead, the maximum spin state possible for the cleaved structure is $S = 3$ involving low-spin Mn^{III} centers.

Comparison of *μ*-oxo- and Bis(*μ*-oxo)-Bridged Structures. It is important to understand what factors lead to stabilization of the peroxide bridge in the current model system $[Mn^{III}_2(\mu\text{-}O)(\mu\text{-}O_2)(NH_3)_8]^{2+}$ but cleavage of the same bridge in the related $[Mn^{III}_2(\mu\text{-}O)_2(\mu\text{-}O_2)(NH_3)_6]^{2+}$ complex. In the latter, the Mn ions are in an approximately octahedral environment with the two oxo bridges and an oxygen of the peroxo bridge comprising one triangular face of the octahedron. Recent papers describing the electronic structure of $[Mn^{IV}_2(\mu\text{-}O)_2(\mu\text{-}O_2)(NH_3)_6]^{2+}$ have emphasized the fact that oxo and peroxo donors exert a strong ligand field.[9,12,18−20] As a consequence, reduction to the Mn^{III} oxidation state, without relaxation of the structure, leads to a low-spin Mn^{III} configuration.[18] In $[Mn^{III}_2(\mu\text{-}O)(\mu\text{-}O_2)(NH_3)_8]^{2+}$, the Mn ions again possess approximately octahedral coordination, but now there is only a single oxo bridge and the axial coordination sites are occupied by ammonia ligands. Although the mixed oxo and ammonia coordination around the Mn centers will undoubtedly induce splitting of the former octahedral e_g orbitals, a Jahn−Teller effect is possible due to the approximate degeneracy of these orbitals. The combination of the weaker ligand field and the ability of the complex to distort along the axial direction due to a Jahn−Teller effect leads to a high-spin Mn^{III} configuration and stabilization of the peroxo bridge across the Mn centers. This is apparent from Figure 5, where a dramatic stabilization of the d_{z^2} orbital occurs relative to $[Mn^{IV}_2(\mu\text{-}O)_2(\mu\text{-}O_2)(NH_3)_6]^{2+}$. In contrast, the combination of the tribridged geometry and the large ligand field exerted by the peroxo and two oxo ligands in $[Mn^{III}_2(\mu\text{-}O)_2(\mu\text{-}O_2)(NH_3)_6]$ ensures that there is no bond axis along which the complex can distort sufficiently to stabilize the d_{z^2} orbital. Hence, the Mn^{III} centers are low spin and the transition from the peroxo-bridged structure, $[Mn^{III}_2(\mu\text{-}O)_2(\mu\text{-}O_2)(NH_3)_6]$, to the cleaved structure, $[(Mn^{IV}O)_2(\mu\text{-}O)_2(NH_3)_6]$, occurs spontaneously without any apparent energy barrier.

Differences in the magnitude of the Jahn−Teller effect can also explain why the lowest energy structure for $[Mn^{III}_2(\mu\text{-}O)(\mu\text{-}O_2)(NH_3)_8]^{2+}$ has the peroxo O−O bond intact whereas the closely related structure $[Mn^{III}_2(\mu\text{-}O)(\mu\text{-}O_2)(NH_3)_6(H_2O)_2]^{2+}$ is calculated to have a cleaved O−O bond. In the latter complex, the presence of a water ligand in one of the equatorial coordination sites on each Mn center amplifies the difference between the axial and equatorial ligand fields. This in turn increases the low-symmetry splitting of the parent octahedral e_g orbitals, thus reducing the magnitude of the Jahn−Teller effect relative to $[Mn^{III}_2(\mu\text{-}O)(\mu\text{-}O_2)(NH_3)_8]^{2+}$.

The concept that the stability of the Mn^{III}_2 oxidation state with an intact peroxo bridge is due to the Jahn−Teller stabilization of the d_{z^2} orbitals is consistent with redox studies on a series of dimers with a $[Mn_2(\mu\text{-}O)_2]^{n+}$ core. Glerup and co-workers[35,37] showed that, with appropriate ligand substitution, steric effects could lead to an elongated $Mn-N_{ax}$ distance which in turn gave rise to substantial shifts in the $Mn^{III}Mn^{III} \rightarrow Mn^{III}Mn^{IV}$ and $Mn^{III}Mn^{IV} \rightarrow Mn^{IV}Mn^{IV}$ redox potentials and stabilization of the $Mn^{III}Mn^{III}$ oxidation state over that of $Mn^{IV}Mn^{IV}$.

Trimer Model. The calculations on the model dimer system $[Mn^{III}_2(\mu\text{-}O)(\mu\text{-}O_2)(NH_3)_6(H_2O)_2]^{2+}$ have gone a long

Table 3. Calculated Structural Parameters for the Model Trimer Complex $[Mn_3(\mu_3\text{-}O)(\mu\text{-}O_2)(O_2CH)_2(NH_3)_6]^{2+}$ [a]

	$S = 5$	$S = 6$	expt
$Mn_{1-}Mn_2$/Å	3.36	3.33	3.14(4)
O−O/Å	1.94	1.39	1.6(1)
$Mn_{1,2-}O$/Å	2.01	2.07	1.9(1)
$Mn_{3-}O$/Å	2.10	1.90	1.8(1)
$Mn_{1,2-}O_2$/Å	1.68	1.88	1.7(1)
$Mn_{1,2-}N_{ax}$/Å	2.17	2.39	2.4(1)
	2.11	2.31	2.2(1)
$Mn_{3-}N_{ax}$/Å	2.32	2.39	2.3(1)
	2.32	2.39	2.1(1)
$Mn_{1,2-}N_{eq}$/Å	2.24	2.29	2.1(1)
$Mn_{3-}N_{eq}$/Å	2.45	2.21	2.2(1)
$Mn_{1,2-}O_{eq}$/Å	2.09	2.01	2.0(1)
$Mn_{3-}O_{eq}$/Å	2.06	2.07	2.1(1)
energy/eV	−249.707	−249.876	
$\rho_{spin}(Mn_{1,2})$	2.81	3.99	
$\rho_{spin}(Mn_3)$	4.43	4.05	
$\rho_{spin}(O)$	−0.06	0.01	
$\rho_{spin}(O-O)$	0.01	−0.15	

[a] Mn_1 and Mn_2 are connected by the μ-peroxo bridge. The experimental data refer to the corresponding structural parameters in $[Mn_3(\mu_3\text{-}O)(\mu\text{-}O_2)(AcO)_2(dien)_3]^{2+}$.[26] ρ_{spin} refers to the spin density on the relevant atom.

way towards rationalizing the stability of the peroxide bridge in complexes possessing a $[Mn^{III}(\mu\text{-}O)(\mu\text{-}O_2)Mn^{III}]$ core over those having a $[Mn^{III}(\mu\text{-}O)_2(\mu\text{-}O_2)Mn^{III}]$ core. However, although the structurally characterized trimer $[Mn^{III}_3(\mu_3\text{-}O)(\mu\text{-}O_2)(AcO)_2(dien)_3]^{2+}$ contains the former core, the measured peroxo O−O distance of 1.6(1) Å is certainly indicative of significant weakening of the O−O bond. It is therefore relevant to ask whether geometrical constraints arising from the bridging architecture of the trimer prevent the O−O bond from undergoing cleavage. To address this problem, DFT calculations were undertaken on the model trimer $[Mn^{III}_3(\mu_3\text{-}O)(\mu\text{-}O_2)(HCO_2)_2(NH_3)_9]^{2+}$.

The results of the geometry optimization of the model trimer complex employing pseudo-C_2 symmetry are presented in Table 3 for the maximum spin states of $S = 5$ and $S = 6$ which arise from coupling between the three Mn centers with all spins aligned parallel. Calculations were also performed on a number of different broken-symmetry states, but in all cases convergence of the associated structures proved problematic. The $S = 6$ state involves coupling of three high-spin Mn^{III} centers ($S_1 = S_2 = S_3 = 2$) for which the peroxide bridge is intact whereas the $S = 5$ state results from the coupling of two Mn^{IV}═O entities ($S_1 = S_2 = 3/2$) and a high-spin Mn^{III} ($S_3 = 2$) ion associated with a cleaved peroxide bridge structure. The coupling schemes for both states are depicted in Figure 8.

The data in Table 3 reveal that the $S = 6$ state is the lowest energy structure but only by approximately 0.2 eV. Analogous to the $S = 4$ state of the dimer model, the calculated O−O distance of 1.39 Å indicates that the peroxo bridge is intact. Most of the structural parameters are similar to those calculated for the dimer $S = 4$ state with the exception of the Mn−O distance which has increased by over 0.2 Å. This lengthening, and the fact that the $Mn_{3-}O$ bond lengths in the $S = 5$ and $S = 6$ states also differ by 0.2 Å, indicates that the third Mn center strongly influences the bonding associated with the μ_3-oxo bridge structure. The calculated

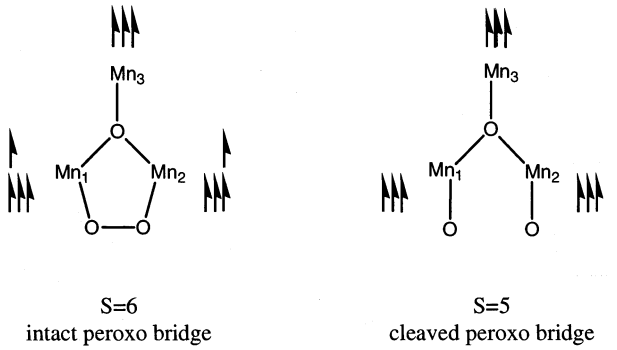

Figure 8. Spin coupling schemes giving rise to the $S = 6$ and $S = 5$ states of the model trimer $[Mn^{III}_3(\mu_3\text{-}O)(\mu\text{-}O_2)(HCO_2)_2(NH_3)_9]^{2+}$.

spin densities of 3.99, 3.99, and 4.05 for Mn_1, Mn_2, and Mn_3 in the $S = 6$ state confirm the assignment of all three metal oxidation states as high-spin Mn^{III}. However, the small unpaired spin density of 0.15 on the peroxo O atoms suggests that the O−O bond is weakened slightly.

In the $S = 5$ state, the O−O distance has increased to 1.94 Å, corresponding to a cleaved O−O bond, and the calculated spin densities of 2.8 on Mn_1 and Mn_2 are indicative of Mn^{IV} ions, analogous to the structure calculated for the dimer $S = 3$ state. Apart from the higher energy calculated for the $S = 5$ state, a cleaved peroxide bridge structure for the trimer can be ruled out on the basis of the calculated O−O bond length (approximately 0.35 Å longer than observed) and also from the fact that $Mn-N_{eq}$ bond distance is calculated to be longer than the $Mn-N_{ax}$ distance, in conflict with the experimental structure. Indeed, on the basis of the model dimer calculations, the elongation of the axial Mn−N bonds (due to a pseudo-JT effect) observed in the experimental structure should be interpreted as evidence for an intact peroxo bridge. For the $S = 6$ state, elongation of axial Mn−N bonds is certainly evident but the difference between the calculated $Mn-N_{ax}$ and $Mn-N_{eq}$ bond distances is about 0.1 Å smaller than those determined for the model dimer implying that the Jahn−Teller effect is reduced in the model trimer. This reduction cannot be attributed to a weakening of the peroxo O−O bond relative to the dimer $S = 4$ state as the calculated O−O bond is actually 0.04 Å shorter in the trimer. Instead, on the basis of the calculated Mn−O and $Mn-N_{eq}$ bond distances which are approximately 0.2 and 0.1 Å longer in the model trimer, it appears that the Jahn−Teller effect is also operating in the $N_{eq}-Mn-O$ direction which in turn moderates the elongation along the $Mn-N_{ax}$ axis. This elongation along the $N_{eq}-Mn-O$ direction, however, is not evident in the experimental structure, presumably due to the steric constraints imposed by the tridentate nature of the dien ligands.

On the basis of the above calculations, it would appear that the bridging architecture of the trimer does not prevent the peroxide bridge from cleaving. Instead, given the small energy differences between the cleaved and uncleaved structures, significant flexibility in the peroxo O−O distance is to be expected, accounting for the somewhat lengthened O−O distance in the observed structure.

Conclusion

The DFT calculations reported in this work indicate that the stability of the peroxo bridge in oxomanganese clusters containing a μ-oxo Mn^{III}_2 core compared to those possessing a bis(μ-oxo) Mn^{III}_2 in which the peroxo O−O bond is cleaved can be attributed to a Jahn−Teller effect. The resulting elongation of the Mn−N_{ax} bonds perpendicular to the Mn_2-(μ-O)(μ-O_2) plane and consequent stabilization of the d_{z^2} orbital leads to high-spin Mn^{III} ions where the absence of minority-spin t_{2g} electrons prevents delocalization of electron density from the Mn centers to the O−O σ^* orbital of the peroxide ligand. Calculations on both model dimer and trimer complexes show that the energetic differences between the cleaved and uncleaved μ-peroxo structures is small, the lowest energy structure depending on the nature of the terminal ligands, and consequently, the peroxide bridge is likely to be quite facile.

IC0205740